

Event-chain Monte Carlo for classical continuous spin models

Manon Michel,^{*} Johannes Mayer, and Werner Krauth[†]

Laboratoire de Physique Statistique, Ecole Normale Supérieure / PSL Research University,
UPMC, Université Paris Diderot, CNRS, 24 rue Lhomond, 75005 Paris, France

(Dated: May 24, 2022)

We apply the event-chain Monte Carlo algorithm to classical continuum spin models on a lattice and clarify the condition for its validity. In the two-dimensional XY model, it outperforms the local Monte Carlo algorithm by two orders of magnitude, although it remains slower than the Wolff cluster algorithm. In the three-dimensional XY spin glass model at low temperature, the event-chain algorithm is far superior to the other algorithms.

Keywords: Markov-chain Monte Carlo algorithms; XY model; spin glasses; event-chain Monte Carlo; lifting; global balance condition

INTRODUCTION

Classical and quantum spin models are of fundamental interest in statistical and condensed-matter physics. Spin models are also a crucial test bed for computational algorithms.

An important representative is the model of continuous two-dimensional classical spins of fixed length (rotators) on a two-dimensional lattice. Thirty years ago, the existence and nature of the phase transition in this two-dimensional XY model were highly controversial[1]. The substitution of the traditional local Monte Carlo (LMC) algorithm[2] by Wolff’s spin flip cluster (SFC) algorithm[3] then quickly allowed to clarify that this model indeed undergoes a Kosterlitz-Thouless transition[4, 5], whose temperature is now known to five significant digits [6, 7]. SFC has played a decisive role in understanding the physics of the XY model[8–10], and in arriving at its detailed quantitative description.

SFC and its variants can be implemented for a wide range of models, but they are efficient only in a few of them. Particularly frustrating is the case of the three-dimensional XY spin glass model, where the algorithm loses all its power[11, 12]. For this much studied spin glass model, our understanding today resembles the one of the XY model before the revolution triggered by the cluster algorithms. Clearly, there still is a great need for more powerful algorithms for classical and quantum spin models.

Today’s Markov-chain Monte Carlo algorithms generally follow the conventional paradigm based on three principles: 1/ Each move represents a finite change of the configuration. It is independent of the previous move, and depends only on the configuration itself. 2/ The algorithm satisfies the detailed-balance condition. 3/ The decision whether a proposed move is accepted is based on the change in energy, using the Metropolis acceptance rule or the heat-bath condition[2, 13].

In the present work, we show that the novel event-chain Monte Carlo (ECMC) paradigm[14–16], that has already been very successful in particle systems [17–20],

can also be applied to the XY model and the XY spin glass model. The paradigm breaks all three principles of the conventional Markov-chain scheme: Moves are infinitesimal rather than finite, although an event-driven scheme allows to recover finite displacements[16]. In one-dimensional systems, the moves do not change with time. In multidimensional systems, moves persist on long time scales. This is achieved within the Markov-chain scheme through additional “lifting” variables[15, 21]. In addition, ECMC violates detailed balance and only satisfies the weaker global balance condition (cf. [22–26]). Finally, the decision on future moves is based on the change in pair energies, rather than the change in total energy. This is achieved by replacing the standard Metropolis algorithm by its recently introduced factorized variant[15].

For the two-dimensional XY model at the critical point, we find that ECMC is about 100 times faster than LMC, although the presence of a slow time scale in auto-correlation functions makes that it is not as fast as SFC. In the low-temperature phase of the three-dimensional XY spin glass model, where SFC is known to be inefficient, ECMC clearly outperforms LMC.

FROM LOCAL MONTE CARLO TO THE “EVENT-CHAIN” ALGORITHM

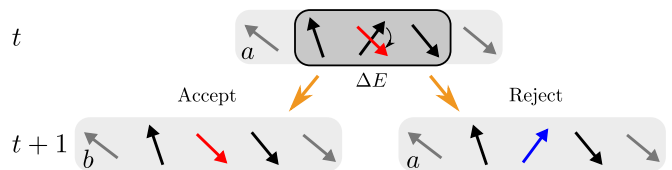


FIG. 1. LMC move for the one-dimensional XY model. *Upper panel*: Configuration at time t and proposed displacement $\Delta\phi$ of a randomly chosen spin, corresponding to an energy change ΔE . *Lower panel*: Possible configurations at time $t + 1$: The proposed move is accepted with probability $\min(1, \exp(-\beta\Delta E))$ (left) and rejected otherwise (right).

In the two-dimensional ferromagnetic XY model of

spins $\mathbf{S}_k = (S_k^x, S_k^y) = (\cos \phi_k, \sin \phi_k)$ on a lattice with sites $i = 1, \dots, N$, and with an energy

$$E = - \sum_{\langle i,j \rangle} J_{ij} \mathbf{S}_i \cdot \mathbf{S}_j = \sum_{\langle i,j \rangle} \underbrace{[-J_{ij} \cos(\phi_i - \phi_j)]}_{E_{ij}}, \quad (1)$$

the coupling constants J_{ij} are all equal to one. The sum $\langle i,j \rangle$ goes over nearest neighbors on the lattice. We refer to the E_{ij} as “pair energies”. The XY model on a two-dimensional square lattice undergoes a phase transition at inverse temperature $\beta = 1.1199$, see ref. [6].

In LMC, one proposes at each time step t a finite move from a configuration a to a configuration b (a rotation by a finite angle $\Delta\phi$ of a spin k), as sketched in Fig. 1. To satisfy detailed balance[13], k is randomly chosen at each time step, and $\Delta\phi$ is sampled from a symmetric distribution around zero, so that $\Delta\phi$ arises with the same probability as $-\Delta\phi$. The proposed move corresponds to an energy change $\Delta E = E_b - E_a$ in Eq. 1, and it is accepted with probability

$$p_{\text{acc}}^{\text{Met}} = \min(1, \exp(-\beta\Delta E)). \quad (2)$$

The exponential in this equation corresponds to the ratio π_b/π_a of the Boltzmann weights of the configurations.

Practically, the move is accepted, and the configuration updated to b , if a uniform random number between 0 and 1 satisfies $\text{ran}(0, 1) < p_{\text{acc}}^{\text{Met}}$ (see [13]). Otherwise, the configuration at time $t+1$ is the same as the one at time t , namely a .

The recently introduced factorized algorithm[15] also satisfies the detailed-balance condition. In this method, the energy-based Metropolis acceptance probability is replaced by a factorized form which separately depends on the pair-energy changes:

$$p_{\text{acc}}^{\text{fact}} = \prod_{\langle k,l \rangle} p_{\text{acc}}^{kl} = \prod_{\langle k,l \rangle} \min(1, \exp(-\beta\Delta E_{kl})). \quad (3)$$

The proposed move $a \rightarrow b$ is accepted with this probability. The factorized algorithm always has a smaller acceptance rate than the conventional one, $p_{\text{acc}}^{\text{fact}} \leq p_{\text{acc}}^{\text{Met}}$ (this will however turn out not to be a problem in ECMC). To implement Eq. 3, one might use a single random number and accept the move if $\text{ran}(0, 1) < p_{\text{acc}}^{\text{fact}}$. We rather accept the move if several independent random numbers satisfy $\text{ran}_{kl}(0, 1) < p_{\text{acc}}^{kl}$ for all pairs k, l . In other words, a move is accepted only if it is pair-accepted by all pairs k, l . This consensus rule is illustrated in Fig. 2. We note that the factorization in Eq. 3 relies on the possibility to cut the hamiltonian into independent pieces. The factorization may also be used to separate different components of the inter-particle potential, as for example the $1/r^6$ and $1/r^{12}$ pieces in the Lennard-Jones potential [15, 19].

The ECMC combines the factorized Metropolis probability with the “lifting” concept of Diaconis et al.[21]

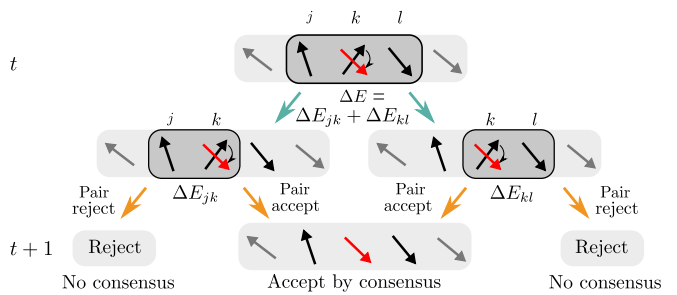


FIG. 2. Factorized Metropolis move. *Upper panel*: Configuration at time t and proposed displacement $\Delta\phi$ of a randomly chosen spin k . *Middle panel*: Factorization into pairs (j, k) and (k, l) . In the factor (j, k) , the move is pair-accepted with probability $\min(1, \exp(-\beta\Delta E_{jk}))$, etc. *Lower panel*: Possible configurations at time $t+1$: The proposed move is either accepted by consensus (i.e. independently by all pairs) or else rejected.

and with the idea of infinitesimal displacements[15]. The term “lifting” refers to the extension of the physical configuration by an additional variable that fixes the proposed move. Written as \hat{k} , it singles out the spin k as the only one that can move, as $\phi_k \rightarrow \phi_k + \Delta\phi$ (see Fig. 3). If the move is accepted, the lifting variable for the next time step $t+1$ is again \hat{k} . If the physical move is rejected, a lifting move takes place and the lifting variable is passed on to the spin l of the pair that rejected the move, and the physical configuration is unchanged. In both cases, the value of $\Delta\phi$ is used again. Note that for infinitesimal $\Delta\phi$, the acceptance probabilities of the physical moves approach one and the rejection probabilities approach zero. Multiple rejections are totally suppressed, and the choice of \hat{l} is unique[15]. At each time step, either a lifting move or a physical move takes place, and ECMC is thus formally rejection-free.

ECMC satisfies the global balance condition in the XY model, as we now show: For simplicity, we consider only two spins and concentrate on a configuration d (see Fig. 3). This configuration can only be reached through a lifting move from a or through a physical move from b . The global-balance condition[13] states that the flow into configuration d must be equal to the flow out of it:

$$\underbrace{\pi_a p(a \rightarrow d)}_{\mathcal{P}(a \rightarrow d)} + \underbrace{\pi_b p(b \rightarrow d)}_{\mathcal{P}(b \rightarrow d)} = \underbrace{\pi_d p(d \rightarrow f)}_{\mathcal{P}(d \rightarrow f)} + \underbrace{\pi_d p(d \rightarrow a)}_{\mathcal{P}(d \rightarrow a)}. \quad (4)$$

Here, $\mathcal{P}(a \rightarrow d)$ represents the probability flow from a to d , etc. For ECMC, the probabilities p in Eq. 4 coincide with the acceptance probabilities: All configurations carry a lifting variable that specifies the spin that may move and the move itself, $\Delta\phi$.

The statistical weight π_a is trivially equal to π_d be-

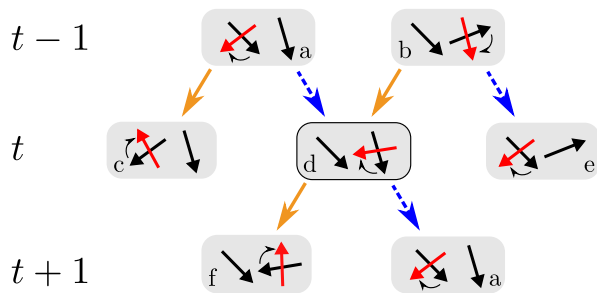


FIG. 3. Lifting approach of ECMC. Physical moves $b \rightarrow d$, $d \rightarrow f$ and $a \rightarrow c$ are by the same infinitesimal angle $\Delta\phi$ in clockwise direction, all others are lifting moves that preserve the physical configuration. Note that $\pi_b = \pi_c$ because of Eq. 1.

cause they differ only by a lifting move. Furthermore, π_c equals π_b , as the two configurations differ only by a global rotation. Writing $\Delta E = E_b - E_d$, we thus find

$$\begin{aligned} \mathcal{P}(b \rightarrow d) &= \pi_b p_{\text{acc}}^{\text{frac}}(b \rightarrow d) = \pi_d p_{\text{acc}}^{\text{frac}}(d \rightarrow b) \\ &= \pi_d \min(1, \exp(-\beta\Delta E)). \end{aligned} \quad (5)$$

Note in this equation that $\pi_b p_{\text{acc}}^{\text{frac}}(b \rightarrow d) = \pi_d p_{\text{acc}}^{\text{frac}}(d \rightarrow b)$, because the factorized transition probabilities satisfy detailed balance. Likewise, the change in energy in going from $a \rightarrow c$ is also ΔE and $p(a \rightarrow d) = 1 - p(a \rightarrow c)$. Therefore, the flow $\mathcal{P}(a \rightarrow d)$ satisfies

$$\begin{aligned} \mathcal{P}(a \rightarrow d) &= \pi_a (1 - \min(1, \exp(-\beta\Delta E))) \\ &= \pi_d (1 - \min(1, \exp(-\beta\Delta E))). \end{aligned} \quad (6)$$

It follows that the flow into d , namely the sum of $\mathcal{P}(a \rightarrow d)$ and of $\mathcal{P}(b \rightarrow d)$, equals π_d . As for the flow out of d , it trivially equals π_d because of the conservation of probabilities. It follows that the global balance of Eq. 4 is satisfied. The factorization property and the infinitesimal limit guarantee that the argument carries over to general N (see [15]).

ECMC violates the detailed balance condition $\mathcal{P}(b \rightarrow d) = \mathcal{P}(d \rightarrow b)$: A move $d \rightarrow b$ would be anti-clockwise, yet all moves within ECMC are, by the initial choice of $\Delta\phi$, clockwise. Also, $\mathcal{P}(a \rightarrow d) = 0$, as $E_d > E_f$ and all physical moves from d to f are accepted. Furthermore, for ECMC to be valid, the pair energy must be symmetric (so that $\pi_b = \pi_c$ in Fig. 3). Modified XY models, as described in ref.[27], can also be treated, but more general pair energies require special considerations[28].

ECMC with infinitesimal moves requires a scaling of physical time: In one unit of time, as $\Delta\phi$ goes to zero, an infinite number of physical moves take place, but the number of lifting moves remains finite. In an event-driven approach[15, 16], the algorithmic complexity can be made to scale with the number of liftings: The lifting variable being set to $\hat{\phi}_k$, the angle ϕ_k now rotates clockwise until the “event”, i.e. a lifting move, is produced

through a rejection by a neighbor l . The lifting variable is updated to $\hat{\phi}_l$, ϕ_l rotates clockwise, etc. Effectively, one undergoes an infinite number of Monte Carlo steps, giving a continuous trajectory.

The angle ϕ_k corresponding to the next event is easily sampled: We continue to consider a single pair (k, l) of spins, with the lifting variable $\hat{\phi}_k$. The i -th infinitesimal update of ϕ_k is noted as the move $i-1 \rightarrow i$ and the weight of the configuration $(\phi_i = \phi_k + i\Delta\phi, \phi_l)$, π_i . The probability $p_{\text{event}}(0 \rightarrow n)$ to accept n subsequent physical moves and then to reject the $n+1$ st physical move is

$$p_{\text{event}}(0 \rightarrow n) = p_{\text{acc}}(0 \rightarrow 1) \cdots p_{\text{acc}}(n-1 \rightarrow n) [1 - p_{\text{acc}}(n \rightarrow n+1)]. \quad (7)$$

The j th term in this expression is $\min(1, \pi_j/\pi_{j-1})$. Supposing for a moment that π_j is monotonously decreasing with j , this gives

$$\begin{aligned} p_{\text{event}}(0 \rightarrow n) &= \frac{\pi_{n-1}}{\pi_0} \left(1 - \frac{\pi_n}{\pi_{n-1}}\right) \\ &= \frac{-1}{\pi_0} \left. \frac{\partial \pi}{\partial \phi_k} \right|_{\phi_k = \phi_n} d\phi. \end{aligned} \quad (8)$$

This probability is normalized, writing ϕ_{event} the value of ϕ_k at which the event happens:

$$\begin{aligned} -\frac{1}{\pi_0} \int_0^\infty \left. \frac{\partial \pi}{\partial \phi_k} \right|_{\phi_k = \phi_{\text{event}}} d\phi_{\text{event}} \\ = \frac{1}{\pi_0} \int_0^{\pi_0} d\pi_{\text{event}} = 1. \end{aligned} \quad (9)$$

This integral is sampled by [13]

$$\begin{aligned} \pi_{\text{event}} &= \text{ran}(0, \pi_0) \\ \pi_{\text{event}}/\pi_0 &= \text{ran}(0, 1), \end{aligned} \quad (10)$$

which is equivalent to the following sampling of the energy increase:

$$\Delta E(\phi_{\text{event}}) = -[\log \text{ran}(0, 1)]/\beta. \quad (11)$$

Sampling π uniformly between 0 and the present value, π_0 (equivalently, ΔE from its exponential distribution) thus yields the event time, ϕ_{event} (see Fig. 4).

For a non-monotonous probability distribution, all negative energy increments correspond to an acceptance probability 1, and disappear from Eq. 7. The sampling of the energy increase in Eq. 11 turns into the sampling of only the positive energy changes. As shown in Fig. 4, this can be expressed as a function E^* , constructed only from the positive increments of the energy E [16].

For a system of more than one pair of spins, the event times ϕ_{event} for each neighbor of the lifted spin k can be computed independently in view of the factorized probability of Eq. 3, and k turns clockwise up to the earliest

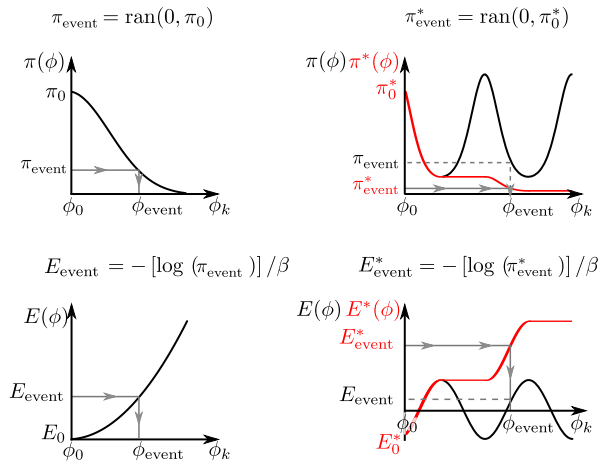


FIG. 4. Event-driven implementation of ECMC for a pair of spins (k, l) . From a starting point $\phi_k = \phi_0$ of weight π_0 and energy E_0 , ϕ_k is updated by infinitesimal moves until $\phi_k = \phi_{\text{event}}$. *Left*: Monotonously decreasing distribution π : The lifting event is sampled as $\pi_{\text{event}} = \text{ran}(0, \pi_0)$. *Right*: General distribution π : $E_{\text{event}}^* - E^*(0) = [-\log \text{ran}(0, 1)]/\beta$.

event (that involves, say, another spin l). The lifting variable is then set to \hat{l} .

It follows from Eq. 7 that all configurations encountered between two events sample the Boltzmann distribution. Any uniform subset of these configurations can be used for averaging observables. A practical choice consists in outputting spin configurations at regular intervals independent of the occurrence of events.

For the models considered here, we found that the efficiency was not increased by halting and restarting the simulation after fixed displacements. In contrast, switches between moves along the different coordinate axes assure ergodicity in multi-dimensional hamiltonians as they appear in particles systems[14], but also the related Heisenberg model[29].

SIMULATIONS FOR THE TWO-DIMENSIONAL XY MODEL AT THE CRITICAL POINT

In the two-dimensional XY model, we consider the susceptibility χ

$$\chi = \frac{\|\sum \mathbf{S}_k\|^2}{N}, \quad (12)$$

and estimate the convergence properties by the susceptibility autocorrelation function

$$C_\chi(t) = \frac{\langle \chi(t'+t)\chi(t') \rangle - \langle \chi \rangle^2}{\langle \chi^2 \rangle - \langle \chi \rangle^2} \quad (13)$$

at the critical point $\beta = 1.1199$ (see [6]). We suppose that χ is a slow variable of this model. We measure time

in sweeps: For ECMC, one sweep corresponds to $\sim N$ lifting events while for LMC, one sweep corresponds to N attempted moves. For SFC, a sweep denotes $\sim N$ spins added to clusters. The complexity of one sweep is $O(N)$ in the three algorithms and the CPU times used per sweep are roughly comparable.

In Fig. 5, we show the autocorrelation function for the XY model at its critical point, obtained from very long single runs of the algorithms. For LMC and SFC, the decay of the susceptibility autocorrelation function can be described by a single time scale, while for ECMC, it is well described by two time scales:

$$C_\chi(t) \simeq \begin{cases} \exp(-t/\tau^{\text{LMC}}) & (\text{LMC}) \\ \exp(-t/\tau^{\text{SFC}}) & (\text{SFC}) \\ A_0 \exp(-t/\tau_0^{\text{ECMC}}) + \\ A_1 \exp(-t/\tau_1^{\text{ECMC}}) & (\text{ECMC}) \end{cases} \quad (14)$$

For ECMC, this correlation function rapidly decays to $C_\chi \sim 0.1$ on a timescale τ_0^{ECMC} of about 5 sweeps. A slow mode τ_1^{ECMC} then sets in. It presents a $z = 2$ scaling ($\tau_1^{\text{ECMC}} \sim L^2$, with $N = L^2$). As shown on the right panel of Fig. 5, τ_1^{ECMC} is an order of magnitude smaller than τ^{LMC} . Together with the initial rapid decrease, this makes ECMC about one hundred times faster than LMC. However, its dynamical scaling exponent appears to be $z \sim 2$, as for LMC. We notice that in particle systems, ECMC also shows initial ballistic behavior, but then crosses over into slower decay[30].

THREE-DIMENSIONAL XY SPIN GLASS MODEL

We now study ECMC for the three-dimensional XY spin glass model, where the nearest-neighbor coupling constants J_{ij} are drawn from a Gaussian normal distribution of zero mean and unit variance. The algorithm can be formulated as for the ferromagnetic model, and the spins continue to always turn clockwise. We will find evidence that the relaxation dynamics of ECMC differs from the one of LMC. Following [11], we consider the chiral overlap between two independent systems, (1) and (2), with identical coupling constants

$$p_\kappa = \frac{1}{N} \sum_{p=1}^N \kappa_{p\perp\mu}^{(1)} \kappa_{p\perp\mu}^{(2)}, \quad (15)$$

with $\kappa_{p\perp\mu}^{(i)}$ being the chirality at a plaquette p , perpendicular to the axis μ , defined as:

$$\kappa_{p\perp\mu}^{(i)} = \frac{1}{2\sqrt{2}} \sum_{(i,j) \in p} \text{sgn}(J_{ij}) \sin(\phi_i - \phi_j). \quad (16)$$

The sum $\sum_{(i,j) \in p}$ is taken over the four bonds encircling the plaquette p clockwise. By construction, p_κ is a symmetric function about zero. As shown in Fig. 6, ECMC

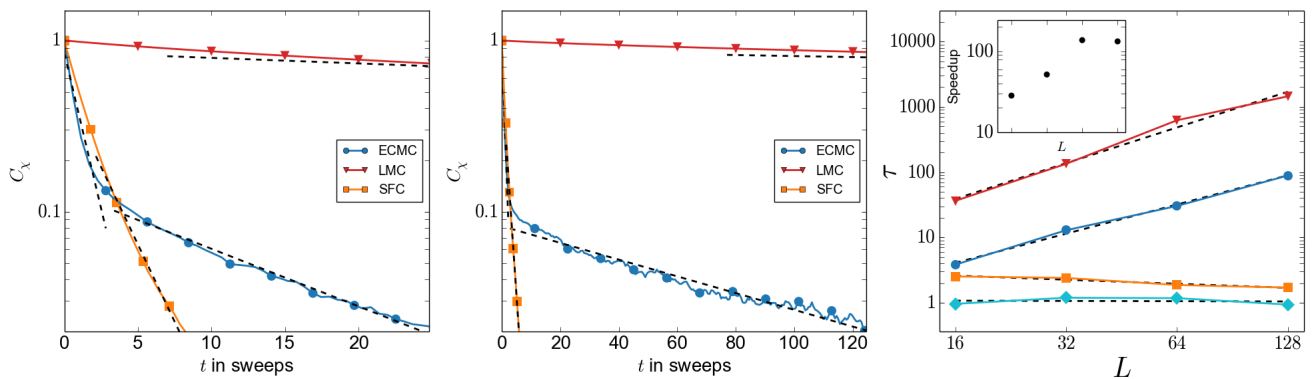


FIG. 5. Autocorrelation function $C_x(t)$ for the two-dimensional XY model at the critical point $\beta = 1.119$ for LMC (red, triangle), ECMC (blue, circle), and SFC (yellow, square). Exponential fits (black, dotted) are as in Eq. 14. Left: $N = 32^2$. Middle: $N = 128^2$. Right: Scaling of the autocorrelation time τ with the system size. Both LMC (red, triangle) and the slow scale of ECMC (dark blue, circle) are compatible with a dynamical scaling exponent $z \sim 2$. Both the fast scale of ECMC (light blue, diamond) and SFC (yellow, square) are compatible with $z \sim 0$. Right Inset: Speedup of ECMC with respect to LMC vs. L .

and LMC agree very well at high temperature. The autocorrelation function of the chiral overlap for LMC and ECMC, shown in Fig. 6, gives at high temperature a size-independent speedup by a factor ~ 5 of ECMC.

The phase diagram of the three-dimensional XY spin glass model at low temperature (with the possible existence of separate spin-glass and chiral-glass phases) is still being debated. We consider $\beta = 3.636$, which may be the locus of the spin glass transition [12], or below it, near the transition [31, 32]. At this temperature, ECMC exhibits a striking advantage over LMC in one third of samples of size $N = 6^3$, where it explores the configuration space more easily, without using parallel tempering [33]. A typical example of a symmetric chiral overlap distribution profile after 10^6 sweeps (symmetric for ECMC, but not for LMC) is shown in Fig. 7, together with the corresponding autocorrelation function. For larger systems, the speedup of ECMC with respect to LMC seems to increase, but already for 10^3 systems, ECMC no longer equilibrates at $\beta = 3.636$.

CONCLUSION

In conclusion, we have applied in this work the recent event-chain algorithm to classical spin models, and obtained a considerable algorithmic speed-up with respect to the local Monte Carlo algorithm for the two-dimensional XY model at its critical point. The new method appears very general, as we also obtained clear acceleration for the three-dimensional XY spin glass model at low temperature. It will be interesting to see how well the event-chain algorithm couples with the traditional acceleration methods, as for example the parallel tempering method, or the overrelaxation approaches that

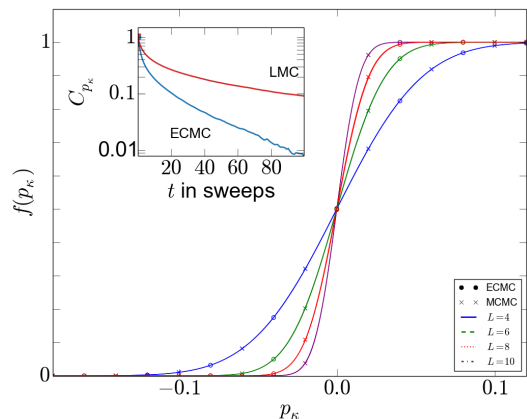


FIG. 6. Cumulative distribution of the chiral overlap p_κ for the three-dimensional XY spin glass model for $N = 4^3, 6^3, 8^3, 10^3$ at $\beta = 1.5$, in the high-temperature phase (single samples). Inset: Autocorrelation function $C_{p_\kappa}(t)$ for $N = 6^3$ from LMC (red, triangle) and ECMC (blue, circle).

have been much used for spin glasses.

ACKNOWLEDGMENTS

We thank K. Hukushima for discussion, and for sharing information about closely related work in his group on the three-dimensional Heisenberg model[29].

This work was granted access to the HPC resources of MesoPSL financed by the Region Ile de France and the project Equip@Meso (reference ANR-10-EQPX-29-01) of the programme Investissements d'Avenir supervised by the Agence Nationale pour la Recherche.

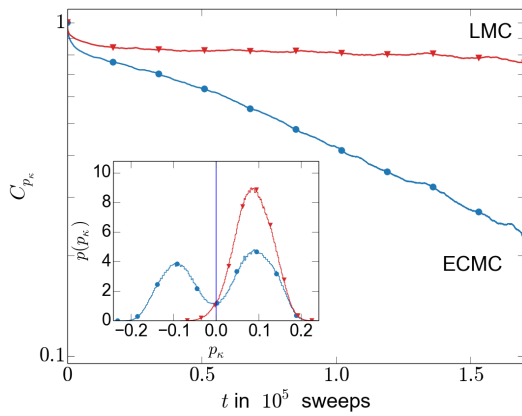


FIG. 7. Chiral overlap autocorrelation function from ECMC and LMC at $\beta = 3.636$ for a given sample at $N = 6^3$. *Inset*: Distributions of p_κ after 10^6 sweeps for the two algorithms in the same sample. Note the nearly symmetric distribution for ECMC.

* manon.michel@ens.fr

† werner.krauth@ens.fr

- [1] E. Seiler, I. O. Stamatescu, A. Patrascioiu and V. Linke, *Nucl. Phys. B* **305**, 623 (1988).
- [2] N. Metropolis, A. W. Rosenbluth, M. N. Rosenbluth, A. H. Teller and E. Teller, *J. Chem. Phys.* **21**, 1087 (1953).
- [3] U. Wolff, *Phys. Rev. Lett.* **62**, 361 (1989).
- [4] M. Hasenbusch, M. Marcu, and K. Pinn, *Physica A* **208**, 124 (1994).
- [5] W. Janke, K. Nather, *Phys. Rev. B* **48**, 7419 (1993).
- [6] M. Hasenbusch, *J. Phys. A: Math. Gen.* **38** 5869-5883 (2005).
- [7] Y. Komura and Y. Okabe, *J. Phys. Soc. Jpn.* **81** 113001 (2012).
- [8] J. M. Kosterlitz and D. J. Thouless, *J. Phys. C* **6**, 1181 (1973); J. M. Kosterlitz, *J. Phys. C* **7**, 1046 (1974).
- [9] J. V. José, L. P. Kadanoff, S. Kirkpatrick and D. R. Nelson, *Phys. Rev. B* **16**, 1217 (1977).
- [10] D. J. Amit, Y. Y. Goldschmidt and G. Grinstein, *J. Phys. A: Math. Gen.* **13** 585 (1980).
- [11] H. Kawamura and M. S. Li, *Phys. Rev. Lett.* **87**, 187204 (2001).
- [12] T. Obuchi and H. Kawamura, *Phys. Rev. B* **87**, 174438 (2013).
- [13] W. Krauth, *Statistical Mechanics: Algorithms and Computations*, Oxford University Press (2006).
- [14] E. P. Bernard, W. Krauth, and D. B. Wilson, *Phys. Rev. E* **80**, 056704 (2009).
- [15] M. Michel, S. C. Kapfer, and W. Krauth, *J. Chem. Phys.* **140**, 054116 (2014).
- [16] E. A. J. F. Peters and G. de With, *Phys. Rev. E* **85**, 026703 (2012).
- [17] E. P. Bernard and W. Krauth, *Phys. Rev. Lett.* **107**, 155704 (2011).
- [18] M. Isobe and W. Krauth, *J. Chem. Phys.*, to appear (2015).
- [19] S. C. Kapfer and W. Krauth, *Phys. Rev. Lett.* **114**, 035702 (2015).
- [20] T. A. Kampmann, H. H. Boltz, and J. Kierfeld, *J. Comp. Phys.*, **281**, 864 (2015).
- [21] P. Diaconis, S. Holmes, and R. M. Neal, *Annals of Applied Probability* **10**, 726 (2000).
- [22] K. S. Turitsyn, M. Chertkov, and M. Vucelja, *Physica D* **240**, 410-414 (2011).
- [23] H. Suwa and S. Todo, *Phys. Rev. Lett* **105**, 120603 (2011).
- [24] H. C. M. Fernandes and M. Weigel, *Comput. Phys. Commun.* **182**, 1856 (2011).
- [25] Y. Sakai and K. Hukushima, *J. Phys. Soc. Japan* **82**, 064003 (2013).
- [26] A. Ichiki and M. Ohzeki, *Phys. Rev. E* **88**, 020101 (2013).
- [27] E. Domany, M. Schick, and R. H. Swendsen, *Phys. Rev. Lett.* **52**, 1535 (1984).
- [28] M. Michel and W. Krauth, unpublished.
- [29] Y. Nishikawa and K. Hukushima, arXiv: 1508.05661 (2015).
- [30] S. C. Kapfer and W. Krauth, *J. Phys. Conference Series* **454**, 012031 (2013).
- [31] J. H. Pixley and A. P. Young, *Phys. Rev. B* **78**, 014419 (2008).
- [32] F. Romá and D. Domínguez, *Phys. Rev. B.* **89**, 024408 (2014).
- [33] K. Hukushima and K. Nemoto, *J. Phys. Soc. Jpn.* **65**, 1604 (1996).